Journal of Pressure Vessel Technology 136 (2014) 031403

doi:10.1115/1.4026448

The Consequences of Macroscopic Segregation on the Transformation Behaviour of a Pressure-Vessel Steel

E.J. Pickering*
Department of Materials Science & Metallurgy
University of Cambridge
Pembroke Street
Cambridge, CB2 3QZ
Email: ejp57@cam.ac.uk

H.K.D.H. Bhadeshia
Department of Materials Science & Metallurgy
University of Cambridge
Pembroke Street
Cambridge, CB2 3QZ
Email: hkdb@cam.ac.uk

It is important that the material used to produce high-integrity pressure vessels has homogeneous properties which are reproducible and within specification. Most heavy pressure vessels comprise large forgings derived from ingots, and are consequently affected by the chemical segregation that occurs during ingot casting. Of particular concern are the compositional variations that arise from macrosegregation, such as the channels of enriched material commonly referred to as A-segregates. By causing corresponding variations in microstructure, the segregation may be detrimental to mechanical properties. It also cannot be removed by any practically feasible heat treatments because of the large scale on which it forms.

Here we describe an investigation on the consequences of macrosegregation on the development of microstructure in a pressure-vessel steel, SA508 Grade 3. It is demonstrated that the kinetics of transformation are sensitive to the segregation, resulting in a dramatic spatial variations in microstructure. It is likely therefore that some of the scatter in mechanical properties as observed for such pressure vessels can be attributed to macroscopic casting-induced chemical segregation.

1 Introduction

The demand that new nuclear plants be able to operate safely over greater service lives has led to onerous materials requirements, particularly in the case of critical components, such as the reactor pressure vessel (RPV). It is important that the steel used for the construction of the RPV has properties which are reliable, and that any variability in properties is small enough to be consistent with good design.

RPVs comprise large forgings produced from ingots that are hundreds of tonnes in weight. A number of defects can arise during the casting process, and these include the inhomogeneities that are produced due to the segregation of alloying elements over large length scales (centimetres or metres). The occurrence of this macrosegregation is due largely to two principal mechanisms, illustrated in Fig. 1 [1, 2]. The first is interdendritic fluid flow in the mushy zone driven by buoyancy forces. This flow is referred to as *thermosolutal* convection, as it occurs due to dissimilarities in density between the enriched interdendritic liquid and the residual bulk liquid, which arise due to differences in temperature and composition. The second is the sedimentation of solute-poor equiaxed grains from the melt. These grains may have entered the bulk melt due to dendrite-arm detachment or heterogeneous nucleation, and fall to the base of the ingot because they have a higher density than the surrounding liquid.

There are a number defects that can arise due to macrosegregation, including A-segregates, V-segregates and negative base segregation, as illustrated in Fig. 2a. Although it is true that much of the V-segregation and negative base segregation is physically removed by cutting when producing a shell forging, Fig. 2b, the A-segregates remain and manifest in the final component. The A-segregates cannot be removed by any practically feasible homogenisation heat treatments due to the large distances involved. They are characterised as channels of enriched material that can extend roughly parallel to the direction of gravity during solidifica-

*Address all correspondence to this author.

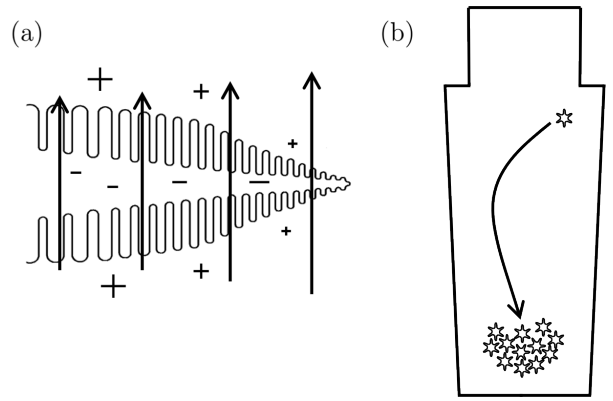

Fig. 1. Prominent macrosegregation mechanisms in steel ingot casting: (a) interdendritic fluid flow caused by thermosolutal convection (+ symbols denote positive segregation, i.e., regions enriched in solute, whilst the − symbols denote depleted regions) and (b) equiaxed grain sedimentation in the melt.

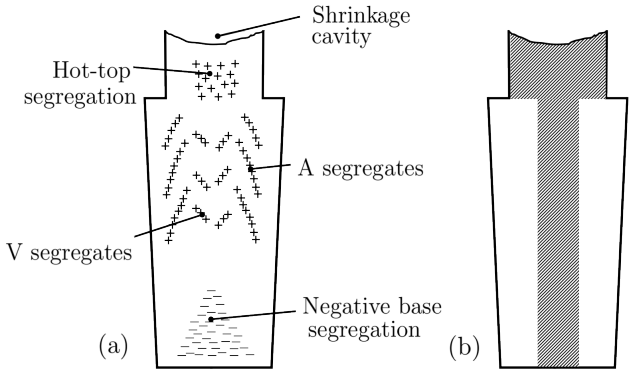

Fig. 2. (a) Different types of macrosegregation typically found in large ingots. Positive segregation is denoted by + symbols representing regions enriched in solute, and negative by − for solute-depleted regions. Similar figures can be found in [1, 5, 6]. (b) Schematic of material removed (shaded) from ingot to produce a typical large shell forging.

tion. As might be expected, the segregated material has been shown to transform into harder microstructures with reduced toughness relative to a homogeneous sample. Indeed, it has been found that in material which has undergone tempering following forging and quenching, the Charpy impact energy of segregated regions can be as little as half that of the non-segregated alloy [3,4]. These defects are therefore of significant concern to vessel designers, particularly if they occur in regions where welds are to be fabricated.

Any change in the chemical composition must influence the thermodynamics and kinetics of phase changes and hence will affect microstructural evolution, with corresponding changes in mechanical properties. Toughness is of particular importance in pressure-vessel applications, and the nature of carbide precipitation appears to be the key controlling microstructural feature in ferritic steels such as SA508 Grade 3. Coarse cementite particles lead to a deterioration in fracture toughness and the ductile-to-brittle transition temperature (DBTT) in SA508 Grade 3, because they act as nucleation sites for the cracks or voids [7–14] (above the DBTT the fracture mechanism is void coalescence, with cleavage below that temperature). Ideally, scatter in fracture energies and DBTTs for a pressure-vessel steel should be minimal, but frequently significant scatter has been observed in SA508 Grade 3 toughness results [15–18]. For the same location, but in different forgings, DBTTs for SA508 Grade 3 have been found to range from 0 to -120°C.

2 Experimental

SA508 Grade 3 material was obtained from a production component, having been cast as part of a large 200-tonne ingot before being forged, quenched and tempered. The solidification time during ingot casting was ∼40 h, and forging was carried out between 1200 and 1300°C (the component was held above 1200°C for over 100 h). The ingot was austenitised between 860 and 880°C for 12 h, before being water quenched and tempered between 635 and 655°C for 10 h. A post-weld heat treatment of 607°C for 19 h was then appplied. Table 1 gives details of the chemical composition of the material investigated, as measured using optical emission spectroscopy and combustion analysis. A plate measuring $20 \times 10 \times 2$ cm was prepared with the normal to its largest surface lying along the longitudinal direction of the ingot (i.e., pointing upwards, parallel to gravity). This was ground to a rough finish before being etched in 5% nitric acid solution, Fig. 3. Areas of positive chemical segregation are clearly observed as dark features. By examining the material found above and below this plate, it was found the segregates extended through a significant vertical distance, indicating they were 'A' type. Cylindrical samples measuring 8 mm in diameter and 12 mm in height were taken from regions with and without A-segregation to assess their phase transformation behaviours (it should be noted that samples containing A-segregates were not comprised purely of these enriched regions, but also some bulk material). A Thermecmastor_Z dilatometer was used for monitoring the progress of phase transformations. Transformation temperatures and phase fractions were determined consistently through a linear-offset method [19, 20]. Following dilatometry, samples were sectioned, metallographically prepared and etched in 2% nital before examination under a Lecia DM2500 M optical microscope. Chemical mapping was performed with a Cameca SX-100 electron probe micro analyser, whilst secondary- and back-scattered electron imaging was carried out with a CamScan MX2600 FEGSEM. Transmission electron microscopy was undertaken using a JOEL 200CX microscope with an accelerating voltage of 200 kV. Thin foils were prepared by electropolishing with a solution of 5% perchloric acid, 25% glycerol and 70% ethanol. The voltage, current and temperature during electropolishing were, 37 V, 26 mA and 10 °C respectively. Vickers hardness measurements were obtained using a Mitutoyo MVK-H2 hardness testing machine, with a load of 2 kg.

Table 1. Composition (wt%) and heat-treatment details, as-received SA508 Grade 3 steel.

Chemistry					
C	Mn	Ni	Mo	Si	Cr
0.184	1.317	0.736	0.488	0.253	0.212
Cu	Al	Co	S	P	V
0.025	0.018	0.012	0.001	0.005	0.003

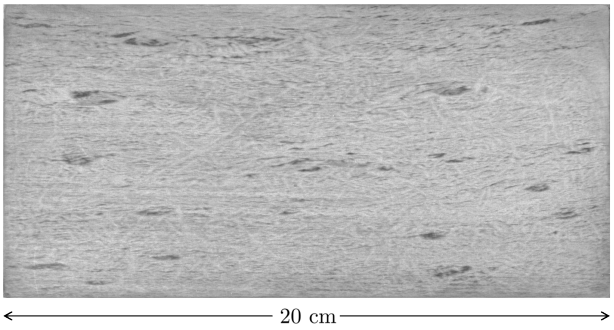

Fig. 3. Section of SA508 Grade 3 forging received, roughly prepared and macroetched. Dark regions are areas of positive segregation. Any horizontal striations are likely caused by the grinding procedure, not macrosegregation.

3 Results

3.1 Dilatometry

Dilatometry measurements were used to determine phase transformation start temperatures and ranges during cooling from austenitisation. All samples were heated to 940°C and held for 30 min before being cooled at 0.1°C s^{-1} to room temperature; the cooling rate chosen to mimic a typical cooling rate in the middle of a thick shell forging during quenching. A summary of the results is shown in Tab. 2. It was immediately evident from the shape of plots of strain against temperature that not only was there a tranformation characteristic of Widmanstätten ferrite or bainite starting at around 550°C, but that other transformations were occurring at higher and lower temperatures, typical of allotriomorphic ferrite and martensite respectively.

Allotriomorphic ferrite formation at high temperature was a common feature in both sets of samples. A higher ferrite start-temperature led not only to an increased quantity of ferrite, but the phase also formed over a larger temperature range. The material with A-segregation showed considerably more variation in measured ferrite phase fractions, with the lowest being $<1\%$ and the highest around 19%. The Widmanstätten ferrite/bainite onset temperature was approximately the same in all samples, but the end of the transformation was consistently lower for samples with A-segregation, giving a greater transformation-temperature range.

Table 2. Dilatometry results for samples with and without A-segregation. The uncertainties in the 'onset' and 'end' temperatures, as well as the ferrite percentages, have been calculated by finding the standard deviation in a dataset which comprised the relevant values for each sample. The error in the 'range' has been found by adding the error in the 'onset' and 'end' temperatures.

	With A-Segregate	Without A-Segregate
Ferrite onset /°C	677 ± 15	672 ± 8
Ferrite end /°C	640 ± 8	640 ± 5
Ferrite range /°C	37 ± 23	32 ± 13
% Ferrite (600°C)	13 ± 6	13 ± 3
Wid./Bain. onset /°C	548 ± 10	553 ± 4
Wid./Bain. end /°C	366 ± 12	380 ± 6
Wid./Bain. range /°C	182 ± 22	173 ± 10
Martensite onset /°C	153 ± 5	153 ± 4

3.2 Optical Microscopy

Optical examination revealed nonuniform microstructures in samples with and without A-segregation, Fig. 4. All samples showed areas with high levels of allotriomorphic ferrite, Fig. 4a-c, which often manifested themselves as clumps or bands spanning hundreds of μm. In material without A-segregation these ferrite-rich areas lay within a relatively homogenous bulk, which appeared to comprise mainly Widmanstätten ferrite, Fig. 4c. In samples which were chosen to include A-segregates, however, these ferrite bands were not only present adjacent to regions of Widmanstätten ferrite, but were also observed very close to A-segregate material, Figures 4a and 4b. In Fig. 4b the transition between enriched A-segregate material, allotriomorphic ferrite, and the Widmanstätten ferrite bulk, can be seen moving from bottom left to top right.

Fig. 4d shows the bulk Widmanstätten ferrite structure. Carbide-rich inter-ferrite regions are evident, which appear practically identical to the dark-etching material observed between allotriomorphic ferrite grains. As shown in Fig. 4f, the structure of the A-segregate material appears to be finer than the Widmanstätten bulk, and blocks of material can be distinguished, separate from the ferritic grains and fine interlath structures, to which etching has given a slightly duller tone.

3.3 Electron Microscopy

The microstructures observed above were investigated at a finer scale using scanning electron microscopy (SEM). Fig. 5a shows the coarse laths of Widmanstätten ferrite, which are free from intragranular precipitation, found in the bulk microstructure. Present in both the Widmanstätten

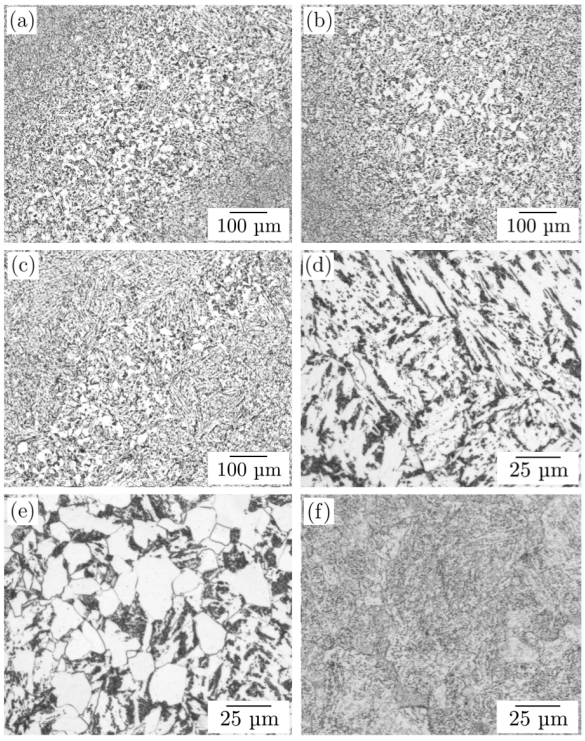

Fig. 4. Optical microscopy. (a) Sample with A-segregation, showing region of allotriomorphic ferrite between two enriched areas. (b) Shows the transition from enriched material, ferrite and widmanstätten ferrite. (c) Region of material without evidence of a-segregation showing band of ferrite within upper-bainite bulk. (d), (e) and (f) show the widmanstätten ferrite, allotriomorphic ferrite and positively-segregated microstructures respectively.

bulk and allotriomorphic microstructures were blocky regions of material, as highlighted in Fig. 5b. These were also present in A-segregate material, in far greater quantity, see Fig. 5c. These regions appeared bright in back-scattered electron images, Fig. 5d, indicating greater enrichment in heavy elements (i.e., nickel, molybdenum) and/or a difference in phase relative to the surrounding material. In many instances, as shown to the the left of Fig. 5c, they also appear to have partially decomposed into a very fine microstructure. These observations are consistent with the blocky regions being retained austenite-martensite islands, and the fine microstructure being bainitic.

TEM analysis showed clearly that the ferritic laths present in the bulk material were Widmanstätten in nature (being too coarse and clean of carbides for bainite), and that the inter-ferrite microstructure was most likely lower bainite with coarse carbides (as opposed to any type of pearlite - more evidence in support of this will be presented at a later date), Fig. 6. Finer lower bainite and twinned martensite was found in A-segregate material.

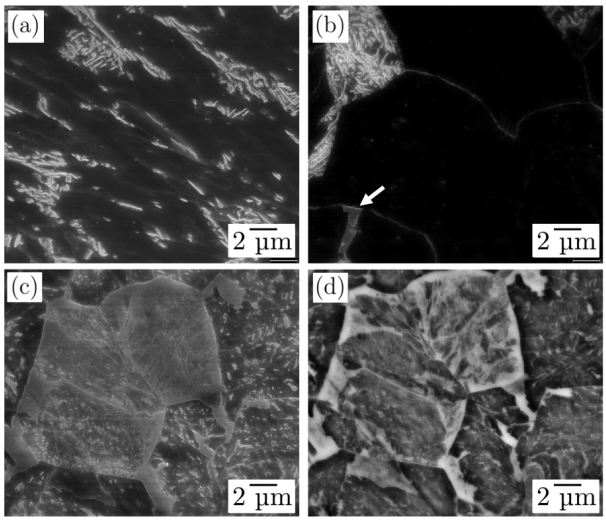

Fig. 5. Scanning electron microscopy: (a) secondary-electron image of enriched region, and (b) corresponding back-scattered electron image. (c) and (d) are secondary-electron images of the allotriomorphic ferrite and widmanstätten ferrite microstructures, respectively. Blocky areas of retained austenite are evident in (c), and a similar formation is labelled in (b).

3.4 Chemical Analysis

A region of Fig. 4b showing the transition from enriched material to allotriomorphic ferrite to Widmanstätten ferrite was subject to electron-probe microanalysis (EPMA), Fig. 7. It is evident that the alloying elements analysed (Si, Mn and Mo) are most concentrated within the A-segregate and least concentrated in the adjoining allotriomorphic ferrite. The results of broad-beam (40 µm) analyses in each of the three regions are shown in Tab. 3. It is evident that the A-segregate material is enriched in all species, whilst the allotriomorphic ferrite regions are only slightly depleted in comparison to the Widmanstätten bulk. A fine probe size (1 µm) was used to try and determine whether there was a chemistry difference between the blocky martensite-austenite regions and surrounding ferrite in A-segregate material, but no difference could be resolved.

3.5 Hardness

Vicker's hardness measurements were taken from three distinct regions: (i) the bands of allotriomorphic ferrite, (ii) homogeneous matrix material (predominantly Widmanstätten ferrite, but with some allotrimorphic ferrite) and (iii) A-segregate regions. Measurements of (i) and (ii) were taken from all samples, whilst measurements of (iii) could only be taken from samples with A-segregates. Results, given in Tab. 4, show a significant variation in hardness between the three regions.

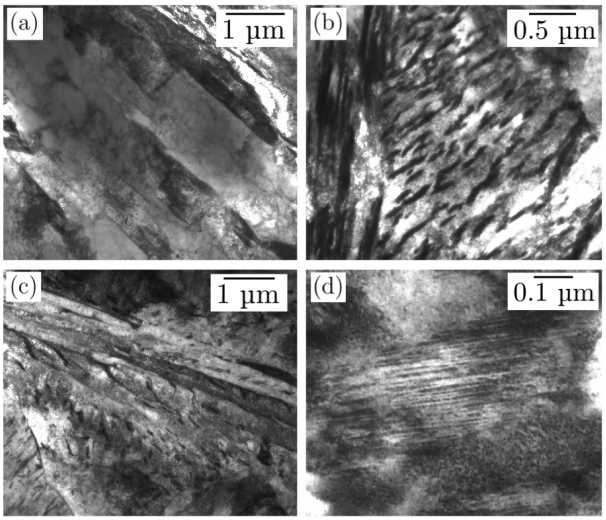

Fig. 6. Transmission electron microscopy: (a) widmanstätten ferrite plates at low magnification, showing carbide-free laths separated by pearlitic regions. (b) Lower bainite colonies with coarse carbides. (c) Thin bainitic laths and extensive carbide precipitation within a-segregated material. (c) Twinned martensite within a martensite-austenite island.

Table 3. The results of EPMA broad-beam spot analysis. Bold numbers are the composition in wt%, standard deviations are given in parentheses and the italicised figure is the value of c/c_0 calculated using the concentrations in Tab. 1 as c_0 values.

Region	Mn	Ni	Mo	Si	Cr
A-Segregate	**1.59** (0.07) *1.21*	**0.86** (0.04) *1.17*	**0.62** (0.06) *1.27*	**0.28** (0.01) *1.10*	**0.26** (0.01) *1.22*
Allotrimorphic Ferrite	**1.26** (0.06) *0.96*	**0.69** (0.03) *0.93*	**0.45** (0.01) *0.93*	**0.24** (0.01) *0.94*	**0.22** (0.01) *1.04*
Widmanstätten Ferrite	**1.28** (0.04) *0.97*	**0.69** (0.02) *0.94*	**0.47** (0.02) *0.95*	**0.24** (0.01) *0.94*	**0.22** (0.01) *1.05*

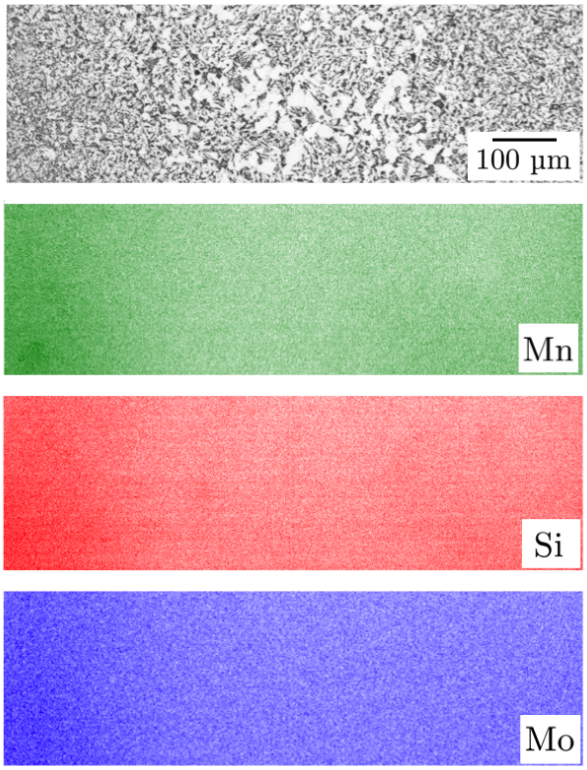

Fig. 7. Qualitative epma mapping showing optical micrograph of region of interest (with A-segregate, allotriomorphic ferrite and widmanstätten ferrite moving bottom left to top right) alongside maps for Si, Mn and Mo.

Table 4. Hardness measurements taken from three distinct microstructures found in material. $\pm$ error in each result is one standard deviation.

Region	Hardness \ HV 2
A-Segregate	318 ± 17
Allotriomorphic Ferrite	210 ± 15
Widmanstätten ferrite	243 ± 10

4 Discussion

Any alloy that enters service in a high-integrity appplication, such as in an RPV, ideally should have homogeneous and predictable properties, yet it is clear that the SA508 Grade 3 material examined in this study exhibited significant and unexpected variability both microstructurally and mechanically. Upper bainite is the preferred microstructure in thick sections of SA508 Grade 3, which provides adequate strength and excellent toughness, but it is evident that the effects of segregation and slow cooling from austenitisation can mean this is not necessarily achieved. Indeed, it is also unclear whether the microstructure of this steel has always been correctly characterised in the past.

4.1 Microstructural Evolution

The results of dilatometry and microscopy suggest that there is a multi-stage evolution of microstructure in the material when the cooling rate from austenitising is $0.1\,^{\circ}\mathrm{C\ s^{-1}}$. First, allotriomorphic ferrite forms between 700 and 650°C in regions depleted of solute. The phase fraction of this ferrite is typically between 0.10 and 0.15, and individual grains are about 20 µm in size. These regions are therefore soft relative to the bulk microstructure. The second transformation

regime occurs with the onset of Widmanstätten ferrite formation, generating the coarse laths predominant in the bulk microstructure. Previous studies have identified similar microstructures (to Fig. 5) as being consistent with upper bainite [7,8,12–14,21], but fine laths of upper bainite, complete with inter-lath carbides, should appear dark under the optical microscope following etching. The coarse ferrite laths observed in this study are clean and free of precipitation, as explicity shown in Figs 5a and 6a. The Widmanstätten ferrite onset temperatures measured were similar in samples both with and without A-segregation because both contained unenriched material (that transformed early on). The end of this transformation was later in samples containing A-segregation due to depressed transformation temperatures in enriched regions.

The formation of allotriomorphic and Widmanstätten ferrite will enrich the remaining austenite in carbon, and the next stage of transformation will be the decomposition of these carbon-rich regions to form lower bainite, with coarse elongated cementite particles, as observed in Figs 5b, and 6c. Finally, any austenite which is still exists will likely decompose into finer bainite, martensite at lower temperatures, or be retained as residual austenite at room temperature. Some blocks of material consistent with martensite-austenite islands have been observed between allotriomorphic and Widmanstätten ferrite grains, but these formations are most prevalent in positively-segregated regions. As observed above, the higher concentration of alloying additions in A-segregate material will lead to the formation of more bainite and martensite-austenite islands. Futher electron-diffraction analysis, to be presented at a later date, will confirm the existence of retained austenite alongside martensite in enriched regions, as well as lower bainite between Widmanstätten and allotriomorphic grains.

4.2 Implications of Results

SA508 Grade 3 is used in service in the quenched and tempered condition, and hence it is essential that the tempering response of the microstructures observed here are realised and related to fracture toughness. Further investigations will confirm the precise development of the three microstructures during further heat treatment, but the following suggestions appear reasonable: Tempering would be expected to decrease the hardness of the bulk Widmanstätten ferrite structure through dislocation removal and precipitate coarsening effects, particularly in the carbide-rich regions between allotriomorphic and Widmanstätten formations. Toughness may initially improve slightly through decreased hardness, but at longer tempering times the formation of coarser cementite could be detrimental to toughness both above and below the DBTT [7, 8, 14, 23]. The allotriomorphic ferrite structure would likely soften also during the tempering, particularly as there is a reduced level of Mo in these regions (a strong carbide forming element), but again carbide coarsening in the regions between ferrite grains could reduce toughness. As for enriched A-segregated areas, it would be reasonable to expect hardness to decrease and toughness to increase on tempering, certainly during the early stages. Firstly, the hardness is likely to drop due to the rapid decomposition of martensite-austenite mixtures into ferrite and cementite. Although there will be some precipitation of fine intragranular Mo_2C, which would be expected to increase strength, this will be more than compensated for by the martensite-austenite decomposition. No significant carbide coarsening will occur during the early stages of tempering, and hence the reduction of hardness would also lead to an increase in toughness.

It is difficult to predict how the toughness of A-segregate material will differ from that of the bulk microstructure. It is true that simply enriching a region in Mo can boost properties (maintain strength, increase toughness and reduce the DBTT) by reducing amount of cementite and replacing with it fine Mo_2C [7, 8, 14], but if there is also high carbon and Mn, then the addition of Mo simply adds strength to the matrix whilst large cementite particles remain, which reduces toughness and the DBTT. An increase in hardness and decrease in toughness over the bulk seems to be the most likely outcome. The presence of larger brittle inclusions in A-segregate material, as well as enrichment in embrittling species (P) may also prove detrimental to toughness, and is being investigated.

The variation in toughness predicted between the three regions may be an underlying factor contributing to the significant scatter often seen in Charpy results from thick-section material [15–18]. Scatter in fracture toughness values should be expected in any ferritic steel because of the statistical nature of finding a suitable carbide ahead of the crack tip to cause fracture [22–25], but the carbide distribution will be significantly affected by the compositional variations highlighted above, and will hence lead to enhanced scatter. Inconsistency in the orientation and location of charpy test specimens relative to features like A-segregates would also likely increase scatter.

Further investigations are needed to assess the response of the material to welding and post-weld heat treatment. It is very likely that a significant amount of martensite-austenite will be formed in A-segregate regions during cooling, but the affect of further microsegregation and the possibility of weld cracking should be examined. Away from A-segregates, a higher cooling rate is more likely to induce a more homogeneous microstructure free from allotriomorphic ferrite. With respect to irradiation hardening susceptibility, it is not clear whether higher levels of alloying elements are necessarily harmful. Some studies suggest that an increase in Ni and Mn can increase irradiation hardening susceptibility [21], although other work suggests that if copper contents are kept low then properties are improved [26].

4.3 Predicting Hardness and DBTT Variability

It would be useful if the effects of segregation on hardness and DBTT could be predicted using general treatments, particularly as it might help explain some of the scatter seen in mechanical test data. For hardness, an extensive study of low-alloy steels as a function of composition and cooling

rate for various microstructures was carried out by Blondeau et al. [27]. Their equations for hardness, replicated in Ion et al. [28], are as follows:

$$H_m = 127 + 949\,\mathrm{C} + 27\,\mathrm{Si} + 11\,\mathrm{Mn} + 8\,\mathrm{Ni} + 16\,\mathrm{Cr} + 21\log V' \quad (1)$$

$$H_b = -323 + 185\,\mathrm{C} + 330\,\mathrm{Si} + 153\,\mathrm{Mn} + 65\,\mathrm{Ni} + 144\,\mathrm{Cr} + 191\,\mathrm{Mo} + (89 + 53\,\mathrm{C} - 55\,\mathrm{Si} - 22\,\mathrm{Mn} - 10\,\mathrm{Ni} - 20\,\mathrm{Cr} - 33\,\mathrm{Mo})\log V' \quad (2)$$

$$H_{fp} = 42 + 223\,\mathrm{C} + 53\,\mathrm{Si} + 30\,\mathrm{Mn} + 12.6\,\mathrm{Ni} + 7\,\mathrm{Cr} + 19\,\mathrm{Mo} + (10 - 19\,\mathrm{Si} + 4\,\mathrm{Ni} + 8\,\mathrm{Cr} + 130\,V)\log V' \quad (3)$$

where H_m, H_b and H_{fp} are the Vicker's hardness values for martensite, bainite and ferrite/pearlite microstructures respectively; V' is the cooling rate in °C h^{-1}; and the compositions are given in wt%. For the composition given in Tab. 1 and cooling rate of 0.1°C s^{-1} , the values for H_m, H_b and H_{fp} are 386, 241 and 182 Hv respectively. The value predicted for H_b is almost identical to that measured for the Widmanstätten bulk (as highlighted above, the Widmanstätten microstructure observed here has often been described as being bainitic in the past, so this discrepancy in label is not an issue). However, the measured hardnesses in the allotriomorphic ferrite or A-segregated regions cannot be matched to either H_m or H_{fp}, even after corrections for the chemistry changes in Tab. 1. This is not unexpected, as the microstructure within these regions will likely be mixed over the area of indentation (indents were over 100 μm across), and it is evident that the regions between ferrite formations in the bulk and depleted material are not filled with pearlite. Clearly then, the general treatment given in Eqn. 1 to 3 is not adequately applicable to the microstructures observed by this study. A model which was able to predict the hardness of mixed microstructures would require a intimate knowledge of continuous-cooling transformation (CCT) behaviour. Ion et al. [28] have already developed such a model for hardness across welds.

For prediction of DBTT, the empirical relations presented by Pickering [29] for various microstructures are a promising starting point. Preliminary calculations using equations (2-17), (2-31) and (2-43) in [29] suggest signficantly different DBTT values can be obtained dependent on the microstructure. Further work on the implementation of these relations needs to be completed, including incorporation of the effects of martensite-austenite regions and elongated carbides on DBTT.

4.4 Origins of Chemical Segregation

There are three segregation mechanisms which have contributed to the microstructural variations observed in this study: microsegregation during solid-state transformation, microsegregation during solidification and macrosegregation during solidification. Firstly, as described above, the partitioning of carbon during the solid-state transformation from austenite to ferrite has led to the formation of islands of pearlite and retained austenite-martensite.

Turning to inhomogeneities at a larger scale in the bulk material, it can be reasonably suggested that the bands of allotriomorphic ferrite present in the microstructure have arisen due to the effects of solidification microsegregation, and subsequent homogenisation during forging. During solidification, a large portion of the solid formed will likely be depleted in solute, Fig. 8, with significant enrichment only occurring in a small fraction of material at the end of the process. On homogenisation of this as-cast concentration profile, solute will rapidly diffuse out of small regions of highly-enriched material, whilst depleted regions at the centre of dendrite arms will more slowly equilibrate (due to concentration gradient effects). This delivers the right conditions for the formation of allotriomorphic ferrite whilst concurrently leaving little evidence of regions enriched by solidification microsegregation - it is apparent that only a small depletion in concentration from the bulk leads to allotriomorphic ferrite formation, whereas the formation of martensite-austenite requires significant enrichment. Hence, some residual depletion at the core of primary and secondary dendrite arms is responsible for the bands of allotriomorphic ferrite (areas of this depletion can be observed in Fig. 3 as well as in [3]). Large dendrite-arm spacings, generated by slow cooling in a large ingot, are responsible for the existence of this residual microsegregation, despite over 100 hours of homogenisation above 1200°C.

It has been evident from the outset of this study that the enriched packets of material present in Fig. 3 were due to A-segregation, but the abrupt change from enriched material to allotriomorphic ferrite, as observed in Figures 4a and 4b, needs to be accounted for. The most likely explanation is that they are residual primary and secondary arm cores that were not remelted away during the generation of the channels. It is unlikely that microsegregation from the enriched A-segregate liquid led to these cores, as they would be more enriched if this was the case. The attribution of allotriomorphic ferrite to the remnants of dendrite arms also goes some way to explain why the levels of ferrite were so variable in samples with A-segregates, as the number of dendrite arms per sample would have been variable.

A-segregates are clearly the most prominent and concerning defect to be found in SA508 Grade 3, and hence their prevention should be a key aim. As stated above, they arise due to the convective flow of enriched liquid in the mushy zone, so minimising the driving force for this would seem like an obvious progression. Within the SA508 specification range, it is likely this could be accomplished by reducing the level of Si and increasing the level of Mo in the alloy [31, 32]. However, a truly rigorous approach would

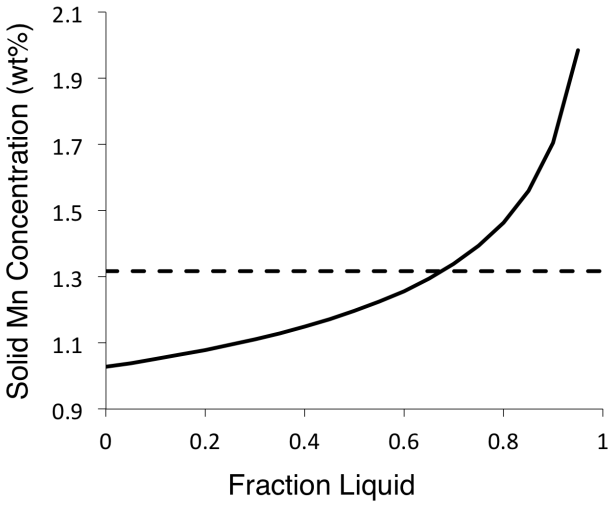

Fig. 8. Plot of solid mn concentration (interfacial value) against fraction solid for the steel examined in the study, under non-equilibrium (Scheil [30]) solidifcation conditions. The dashed line gives the bulk alloy composition. Partition coefficients and liquidus slopes used for calculations were taken from the relevant phase diagrams. Note that the true conditions for solidification of low-alloy steels are likely to be between the ideal equilibrium and non-equilibrium cases.

also account for the effect of this alteration on mushy-zone permeability (i.e., the ease of liquid movement through the dendrites), for example through a Rayleigh-number criterion [32–34], and must also account for the corresponding change in microstructure and properties. Investigations are ongoing.

5 Summary and Conclusions

It has been demonstrated that SA508 Grade 3 production material can exhibit substantial levels of chemical segregation, which can significantly influence phase-transformation behaviour during heat treatment. After austenitisation at 940°C and cooling at a constant 0.1°C s^{-1}, three distinct microstructural regions could be discerned in the material. Within the bulk of the material, a microstructure of Widmanstätten ferrite was predominant, but bands of allotriomorphic ferrite were also common. Chemical analysis revealed that only a slight depletion in solute over the nominal composition led to the generation of allotriomorphic-rich regions, and it was suggested this could arise due to residual microsegregation. A-segregates were readily identified, and the enriched material associated with these produced a mixed microstructure inclusive of bainite, martensite and retained-austenite following the simulated quench.

The mechanical properties of the allotriomorphic ferrite, Widmanstätten ferrite bulk and mixed A-segregate microstructure were very different, and it can be reasonably suggested that a these differences would persist after a tempering heat treatment and impact toughness. Indeed, these variations could contribute to the extensive scatter in toughness measurements so often found in this and similar ferritic alloys. The precise tempering response of these microstructures will be investigated, as will the possibility of reducing levels of A-segregation by altering alloy composition.

Acknowledgements

This work was undertaken as part of a project sponsored by Rolls-Royce Power Engineering plc (Submarines) in collaboration with Sheffield Forgemasters International. We extend our thanks to Professor Lindsay Greer for provision of lab facilities and electron microscopes. The author would like to thank S. Ooi and H. Pous-Romero for helpful discussions.

References

[1] Flemings, M., 1974. *Solidification Processing*. McGraw-Hill, January.

[2] Dantzig, J., and Rappaz, M., 2009. *Solidification*. EPFL Press.

[3] Maidorn, C., and Blind, B., 1985. "Solidification and Segregation in Heavy Forging Ingots". *Nuclear Engineering and Design,* **84**, pp. 285–296.

[4] Druce, S., September 1979. "Investigation of the Homogeneity of Chemical Composition and Mechanical Properties in a Large A508 Class 3 Steel Pressure Vessel Forging". Vol. AERE - R9581.

[5] Taylor, H., Flemings, M., and Wulff, J., 1959. *Foundry Engineering*. Wiley, New York.

[6] Marburg, E., 1953. "Accelerated Solidification in Ingots: Its Influence on Ingot Soundness". *Journal of Metals*, pp. 157–172.

[7] Kim, S., Im, Y., Lee, S., Lee, H., Oh, Y., and Hong, J., 2001. "Effects of Alloying Elements on Mechanical and Fracture Properties of Base Metals and Simulated Heat-Affected Zones of SA 508 Steels". *Metallurgical and Materials Transactions A,* **32A**, pp. 903–911.

[8] Im, Y., Oh, Y., Lee, B., Hong, J., and Lee, H., 2001. "Effects of Carbide Precipitation on the Strength and Charpy Impact Properties of Low Carbon Mn-Ni-Mo Bainitic Steels". *Journal of Nuclear Materials,* **297**, pp. 138–148.

[9] Wang, G., and Chen, J., 1996. "A Comparison of Fracture Behavior of Low Alloy Steel with Different Sizes of Carbide Particles". *Metallurgical and Materials Transactions A,* **27A**, pp. 1909–1917.

[10] Kim, S., Kang, S., Oh, S., Kwon, S., S.Lee, Kim, J., and Hong, J., 2000. "Correlation of the Microstructure and Fracture Toughness of the Heat-Affected Zones of an SA 508 Steel". *Metallurgical and Materials Transactions A,* **31A**, pp. 1107–1119.

[11] Bowen, P., Druce, S., and Knott, J., 1986. "Effects of Microstructure on Cleavage Fracture in Pressure Vessel Steel". *Acta Metallurgica,* **34**, pp. 1121–1131.

[12] Lee, S., Kim, S., Hwang, B., Lee, B., and Lee, C., 2002. "Effect of Carbide Distribution on the Fracture Toughness in the Transition Temperature Region of an SA 508 Steel". *Acta Materialia,* **50**, pp. 4755–4762.

[13] Im, Y., Lee, B., Oh, Y., Hong, J., and Lee, H., 2004. "Effect of Microstructure on the Cleavage Fracture Strength of Low Carbon Mn-Ni-Mo Bainitic Steels". *Journal of Nuclear Materials,* **324**, pp. 33–40.

[14] Kim, S., Lee, S., Im, Y., Lee, H., Kim, S., and Hong, J., 2004. "Effects of Alloying Elements on Fracture Toughness in the Transition Temperature Region of Base Metals and Simulated Heat-Affected Zones of Mn-Mo-Ni Low-Alloy Steels". *Metallurgical and Materials Transactions A,* **35A**, pp. 2027–2037.

[15] Lee, B., Hong, J., Yang, W., Huh, M., and Chi, S., 2000. "Master Curve Characterisation of the Fracture Toughness in Unirradiated and Irradiated RPV Steels Using Full and 1/3-Size Pre-Cracked Charpy Specimens". *International Journal of Pressure Vessels and Piping,* **77**, pp. 599–604.

[16] Beremin, F., 1984. "A Local Criterion for Cleavage Fracture of a Nuclear Pressure Vessel Steel". *Metallurgical Transactions A,* **14A**, pp. 2277–2287.

[17] Kim, J., Kwon, H., Chang, H., and Park, Y., 1997. "Improvement of Impact Toughness of the SA 508 Class 3 Steel for Nuclear Pressure Vessel Through Steel-Making and Heat-Treatment Practices". *Nuclear Engineering and Design,* **174**, pp. 51–58.

[18] Lee, K., Kim, M., Lee, B., and Wee, D., 2010. "Master Curve Characterisation of the Fracture Toughness Behavior in SA508 Gr.4N Low Alloy Steels". *Journal of Nuclear Materials,* **403**, pp. 68–74.

[19] Yang, H.-S., and Bhadeshia, H., 2007. "Uncertainties in Dilatometric Determination of Martensite Start Temperature". *Materials Science and Technology,* **23**(5), pp. 556–560.

[20] Takahashi, M., and Bhadeshia, H., 1989. "The Interpretation of Dilatometric Data for Transformations in Steels". *Journal of Materials Science Letters,* **8**, pp. 477–478.

[21] Lee, B., Kim, M., Yoon, J., and Hong, J., 2010. "Characterisation of High Strength and High Toughness Ni-Mo-Cr Low Alloy Steels for Nuclear Application". *International Journal of Pressure Vessels and Piping,* **87**, pp. 74–80.

[22] Curry, D., and Knott, J., November 1978. "Effects of Microstructure on Cleavage Fracture Stress in Steel". *Metal Science*, pp. 511–514.

[23] Curry, D., and Knott, J., June 1979. "Effect of Microstructure on Cleavage Fracture Toughness of Quenched and Tempered Steels". *Metal Science*, pp. 341–345.

[24] Curry, D., 1980. "Comparison Between Two Models of Cleavage Fracture". *Metal Science*, February, pp. 78–80.

[25] Wallin, K., 1984. "The Scatter in K_IC Results". *Engineering Fracture Mechanics,* **19**, pp. 1085–1093.

[26] Hawthorne, J., 1985. "Composition Influences and Interactions in Radiation Sensitivity of Reactor Vessel Steels". *Nuclear Engineering and Design,* **89**, pp. 223–232.

[27] Blondeau, R., Maynier, P., Dollet, J., and Viellard-Baron, B., 1976. "Mathematical Model for the Calculation of Mechanical Properties of Low Alloy Steel Metallurgical Products: A Few Examples of Its Applications". In Heat Treatment '76, Metals Society.

[28] Ion, J., Easterling, K., and Ashby, M., 1984. "A Second Report on Diagrams of Microstructure and Hardness for Heat-Affected Zones in Welds". *Acta Metallurgica,* **32**, pp. 1949–1962.

[29] Pickering, F., 1992. "Structure-Property Relationships in Steels". In *Constitution and Properties of Steels*, R. Cahn, P. Haasen, E. Kramer, and F. Pickering, eds., Vol. 7 of *Materials Science and Technology: A Comprehensive Treatment*. VCH, pp. 41–94.

[30] Scheil, E., 1942. "Bemerkungen zur Schichtkristallbildung". *Zietschrift fur Metallkunde,* **34**, p. 70.

[31] Suzuki, K., and Taniguchi, K., 1981. "The Mechanism of Reducing "A" Segregates in Steels Ingots". *Transactions ISIJ,* **21**, pp. 235–242.

[32] Beckermann, C. "Private communication".

[33] Beckermann, C., Gu, J., and Boettinger, W., 2000. "Development of a Freckle Predictor via Rayleigh Number Method for Single-Crystal Nickel-Base Superalloy Castings". *Metallurgical and Materials Transactions A,* **31A**, pp. 2545–2557.

[34] Ramirez, J., and Beckermann, C., 2003. "Evaluation of a Rayleigh-Number-Based Freckle Criterion for Pb-Sn Alloys and Ni-Base Superalloys". *Metallurgical and Materials Transactions A,* **34A**, pp. 1525–1536.